JOURNAL OF Materials CHEMISTRY

Structural and physical properties of conducting cation radical salts containing supramolecular assemblies based on *p*-bis(iodoethynyl)benzene derivatives

Hiroshi M. Yamamoto,*[a] Ryoko Maeda,[b] Jun-Ichi Yamaura[b] and Reizo Kato*[a]

[a]*RIKEN (The Institute of Physical and Chemical Research) Hirosawa, Wako-shi, Saitama 351-0198, Japan. E-mail: yhiroshi@postman.riken.go.jp*
[b]*The Institute for Solid State Physics, The University of Tokyo, Kashiwa-shi, Chiba 277-8581, Japan*

Received 10th October 2000, Accepted 22nd January 2001
First published as an Advance Article on the web 22nd February 2001

$(ET)_3Cl(p\text{BIB})$ (ET = bis(ethylenedithio)tetrathiafulvalene, *p*BIB = *p*-bis(iodoethynyl)benzene) salt is a unique organic metal containing supramolecular assemblies based on the *p*BIB molecule and the Cl anion. We newly prepared chloride and bromide ET cation radical salts with the use of di- and tetra-substituted *p*BIB derivatives: 1,4-difluoro-2,5-bis(iodoethynyl)benzene (DFBIB), 1,2,4,5-tetrafluoro-3,6-bis(iodoethynyl)benzene (TFBIB), 1,4-bis(iodoethynyl)-2,5-dimethylbenzene (BIDMB), and *p*-bis(iodoethynyl)benzene-d_4 (*p*BIB-d_4). The effect of substitution has been studied by X-ray structure analyses, tight-binding band calculations, and resistivity measurements. Halide ion replacement as well as deuterium- and difluoro-substitutions do not change the fundamental crystal structure and the metallic behavior, but affect the anisotropy of the electronic structure. On the other hand, the tetrafluoro- and dimethyl-substitutions induce different donor arrangements that lead to semiconducting behaviors.

Introduction

The physical properties of molecular conductors are closely related to their crystal structures, especially their molecular arrangements.[1] In order to develop novel molecular arrangements, the introduction of a supramolecular assembly is one of the most interesting and effective methods, because it can govern the architecture of the crystal. For example, supramolecular assemblies based on intermolecular I···X (X=CN, halide ions) interactions between a donor and an anion have been constructed in several compounds including $(DIETS)_4M(CN)_4$ (DIETS = diiodoethylenedithiodithiadiselenafulvalene, M=Ni, Pd, Pt)[2a] and (IEDT)[$Pd(dmit)_2$] (IEDT = iodoethylenedithiotetrathiafulvalene).[2b] We have focused on this I···X interaction due to its strength and directionality, and have developed a supramolecular system based on iodine-containing neutral molecules. As a result, various types of supramolecular assemblies (one-dimensional (1D) chain, two-dimensional (2D) sheet, and three-dimensional (3D) network) have been constructed in the conductive cation radical salts.[3] These salts show unique crystal and electronic structures.

The organic metal $(ET)_3Cl(p\text{BIB})$ is one of these interesting salts and contains 1D $Cl^-\cdots p\text{BIB}$ chains. The 3 : 1 donor : anion ratio of this salt is achieved by forming the 1D supramolecular assembly with a *ca.* 18.5 Å period, which suggests the possibility of "fractional band-filling control."[3] Indeed, this crystal is the first and the only metallic ET salt where the formal charge of the donor is +1/3. The nature of the cation radical salt with the formal charge of +1/3 is worth further study, especially in comparison with the well-known +1/2-charged systems. In addition, thorough investigation of this system would lead to new superconductors with controlled band filling, since the arrangement of ET molecules in this salt is β-type which is often observed in organic superconductors.

The *p*BIB molecule in the $(ET)_3Cl(p\text{BIB})$ salt can accept a variety of chemical substitutions at the benzene ring. Therefore, substitution on the benzene ring is an effective means of modifying this system. In addition, the chloride ion can be replaced with other halide ions. These chemical modifications would highlight two important effects. At first, they can act as a kind of an "anisotropic" pressure effect, because the introduction of functional groups into the *p*BIB molecule is expected to affect mainly the *inter*-chain interaction while the predominant alteration by halide ion replacement will appear in the chain period (*intra*-chain). In general, the electronic states of molecular conductors are very sensitive to pressure, and many electric phenomena have been found under pressure. Indeed, the first organic superconductor[4] and the highest T_c for an organic superconductor[5] were both realized under pressure. Furthermore, it is a well-known fact that the external pressure effect can be reproduced by chemical modification (internal pressure). For example, in the isostructural anion radical salts $(2,5\text{-}R^1,R^2\text{-}DCNQI)_2Cu$ (DCNQI = *N*,*N*′-dicyanoquinonediimine; R^1, $R^2 = CH_3$, CH_3O, Cl, Br), physical properties are quite sensitive to the choice of the functional groups R^1 and R^2.[6] In particlular, in $(DMe\text{-}DCNQI)_2Cu$ ($R^1 = R^2 = CH_3$), the deuteration induces a drastic metal–insulator transition.[7] Another example is the cation radical salt κ-$(ET)_2CuBr[N(CN)_2]$ where selective deuteration controls the superconducting transition.[8] In these examples, the substitutions work as an application of "chemical" pressure. Compared with hydrostatic pressure, chemical pressure is rather anisotropic and can provide both positive and negative effects. These successful examples of effective chemical pressure encourage us to examine the effects of chemical modifications in our $(ET)_3Cl(p\text{BIB})$ system. It should also be noted that the shape of the calculated 2D Fermi surface of $(ET)_3Cl(p\text{BIB})$ is expected to be sensitive to the intermolecular HOMO···HOMO interactions.[3]

Secondly, structural changes induced by chemical modification will provide information about the guiding principle for supramolecular design. Although the supramolecular framework plays an important role in determining the crystal structure, it does not always provide a unique structure: in

 DOI: 10.1039/b008170l

Table 1 Crystallographic parameters

Crystal	$(ET)_3Cl$ (pBIB)[c]	$(ET)_3Br$ (pBIB) **1**	$(ET)_3Cl$ (DFBIB) **2**	$(ET)_3Br$ (DFBIB) **3**	$(ET)_3Cl$ (pBIB-d_4) **4**	$(ET)_3Br$ (pBIB-d_4) **5**	$(ET)_3Br$ (TFBIB) **6**	$(ET)_2Cl_2$ (BIDMB) **7**
Empirical formula	$C_{40}S_{24}H_{28}ClI_2$	$C_{40}S_{24}H_{28}BrI_2$	$C_{40}S_{24}H_{26}ClF_2I_2$	$C_{40}S_{24}H_{26}BrF_2I_2$	$C_{40}S_{24}H_{24}D_4ClI_2$	$C_{40}S_{24}H_{24}D_4BrI_2$	$C_{40}S_{24}H_{24}BrF_4I_2$	$C_{32}S_{16}H_{24}Cl_2I_2$
Formula weight	1567.36	1611.81	1603.34	1647.80	1571.36	1615.81	1683.78	2492.43
Crystal system	Triclinic	Triclinic	Triclinic	Triclinic	Triclinic	Triclinic	Triclinic	Monoclinic
Space group	$P\bar{1}$	$P\bar{1}$	$P\bar{1}$	$P\bar{1}$	$P\bar{1}$	$P\bar{1}$	$P\bar{1}$	$P2_1/n$
a/Å	10.184(3)	10.187(1)	10.3480(6)	10.361(2)	10.198(1)	10.192(2)	13.180 (1)	23.072 (2)
b/Å	15.578(4)	15.420(2)	15.550(1)	15.373(3)	15.559(2)	15.420(3)	19.128(2)	14.695(1)
c/Å	9.258(3)	9.418(1)	9.2610(5)	9.397(3)	9.296(1)	9.423(2)	12.4640(6)	6.2770(3)
α/deg	99.73(2)	99.83(1)	98.125(5)	98.34(2)	99.634(6)	99.82(2)	105.250(4)	
β/deg	106.87(2)	106.89(1)	107.703(4)	107.54(2)	106.931(7)	106.98(2)	112.817(5)	96.928(5)
γ/deg	76.33(3)	77.21(1)	75.622(3)	76.35(2)	76.581(7)	77.17(2)	82.455(4)	
V/Å^3	1357.7(8)	1371.5(4)	1371.7(1)	1382.5(6)	1364.6(3)	1372.1(5)	2792.9(4)	2112.6(2)
Z	1	1	1	1	1	1	2	2
ρ(calc.)/g cm^{-3}		1.951	1.941	1.979	1.912	1.956	2.002	1.959
ρ(meas.)/g cm^{-3}		1.96(1)	1.95(1)	1.98(1)	1.93(1)	1.95(1)	2.01(1)	1.94(1)
μ/cm^{-1}		28.24	21.50	28.09	21.53	22.56	27.89	24.35
Measured reflections		8318	13318	10718	8410	8527	23512	20422
Independent reflections		7903	5895	7078	5907	8009	10750	5446
σ limit		2	3.00	2	3.00	2	3.00	3.00
GoF		0.97	2.76	1.12	3.99	1.73	2.16	3.54
R,[a] R_w[b]		0.083, 0.220	0.033, 0.041	0.044, 0.167	0.071, 0.081	0.106, 0.294	0.038, 0.042	0.046, 0.052
Device		4-circle	IP	4-circle	IP	4-circle	IP	IP
Refinement on		F^2	F	F^2	F	F^2	F	F

[a] $R=\Sigma\|F_o|-|F_c\|/\Sigma|F_o|$. [b] $R_w=[\Sigma w(F_o^2-F_c^2)^2/\Sigma w(F_o^2)^2]^{1/2}$, $w=[\sigma_c^2(F_o)+(aP)^2]^{-1}$ where $P=(F_o^2+2F_{c^2})/3$, for **1**, **3**, and **5**; $R_w=[\Sigma w(|F_o|-|F_c|)^2/\Sigma w(|F_o|)^2]^{1/2}$, $w=[\sigma_c^2(F_o)+p^2F_o^2/4]^{-1}$, for the others. [c] See ref. 3.

order to accord with all other components in the crystal, the supramolecules themselves also modify their structures depending on the situation. It is therefore important to understand the limitations of the chemical modification that allows the crystal to retain the pristine structure. Such an investigation would yield important information for crystal engineering.

With these points in mind, we introduced fluorine, deuterium, and methyl groups into the pBIB molecule and also examined halide ion replacement. This paper describes the effects of such chemical modifications on the crystal structures and on the electronic structures in the newly obtained cation radical salts.

Results

The galvanostatic oxidation of the donor molecule in the presence of the corresponding neutral molecule and the supporting electrolyte provided $(ET)_3Br$(pBIB) (**1**), $(ET)_3Cl$(DFBIB) (**2**), $(ET)_3Br$(DFBIB) (**3**), $(ET)_3Cl$(pBIB-d_4) (**4**), $(ET)_3Br$(pBIB-d_4) (**5**), $(ET)_3Br$(TFBIB) (**6**), and $(ET)_2Cl_2$(BIDMB) (**7**). Fluoride and iodide salts could not be obtained. The resistivities and relative densities were measured on at least several samples of every batch. Because all the samples from same batch gave identical results within experimental error, we are sure that no polymorph is formed in the sample preparation. X-Ray structure analyses were also performed on these salts at room temperature. In the crystals **1**–**6**, the neutral molecules are coordinated by the anions and form 1D supramolecular assemblies. The distances between the anions and iodine atoms of the neutral molecules are much shorter than the sum of the anion radius of Cl^- (or Br^-) and the van der Waals radius of iodine. Table 1 gives crystal data for these seven salts, **1**–**7**. The small differences between calculated densities and the observed ones (less than 1%) guarantee the accuracy of the crystals' compositions.

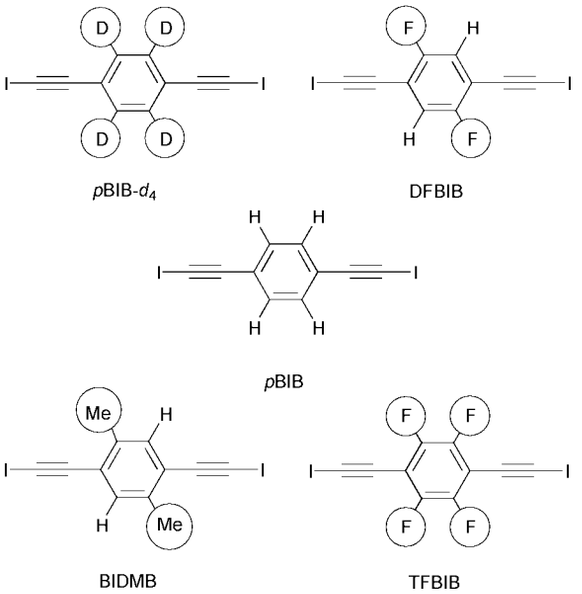

Crystal structures†

$(ET)_3Br$(pBIB) (1); $(ET)_3X$(DFBIB) (X = Cl, 2; Br, 3); $(ET)_3X$(pBIB-d_4) (X = Cl, 4; Br, 5). These five salts are isostructural with $(ET)_3Cl$(pBIB).[3] The crystal structure of **2** is shown in Fig. 1. In the unit cell, there are three donor molecules. Two of them (A and A′) are interrelated by the inversion center and the other one (B) is on the inversion center. Both the anion and the neutral molecule are on the inversion centers. The Cl anions and DFBIB molecules form 1D chains with the period of about 18.5 Å. The inter-chain distance is about 5.0 Å. In addition to the strong $X^-\cdots I$ contacts, the X^- anion also forms weak $CH\cdots X^-$ hydrogen bonds with the H atoms on the benzene rings of the pBIB derivatives ($H\cdots X^- = 2.85$–2.89 Å). The donor arrangements in these salts are β-type.[9] The angle between the longitudinal axes of the donor molecules and the normal of the anion layer is about 40°.

†CCDC reference number 1145/273. See http://www.rsc.org/suppdata/jm/b0/b008170l/ for crystallographic files in .cif format.

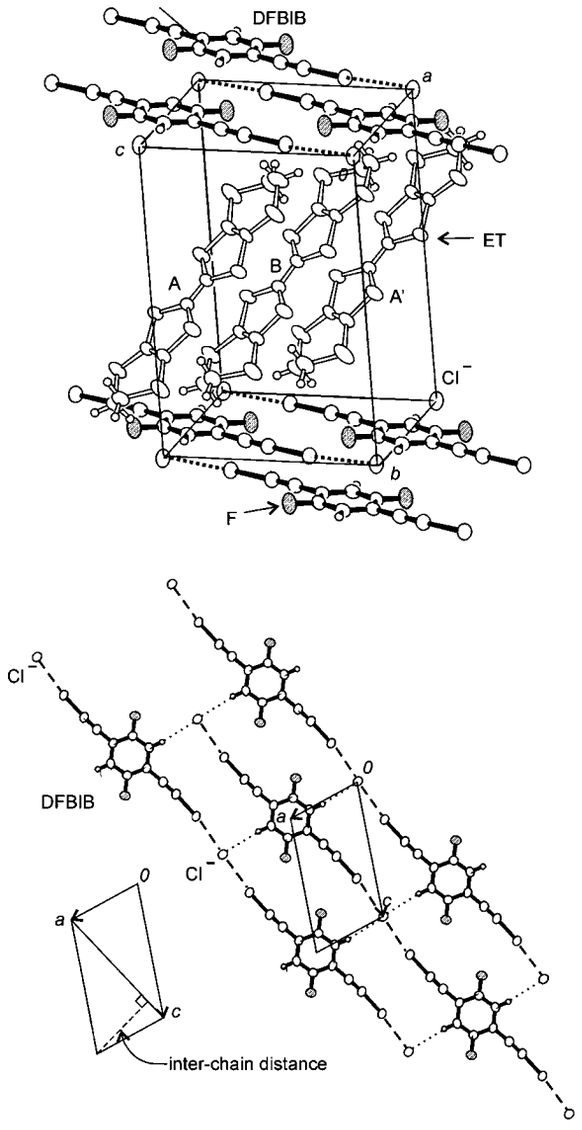

Fig. 1 Crystal packing (upper) and anion layer (lower) in $(ET)_3Cl$(DFBIB) **2**, where dashed lines represent $Cl^-\cdots I$ contacts and dotted lines represent $Cl^-\cdots H$ contacts. F atoms in DFBIB are shaded.

$(ET)_3Br$(TFBIB) 6. The crystal structure of **6** is shown in Fig. 2. The unit cell contains six donor molecules. Two donor pairs (A–A′ and B–B′), each of which is formed by the symmetry operation of inversion, are on general positions. The other two ET molecules (C and D) and the TFBIB molecules are on the inversion centers. Although the Br anions and TFBIB molecules also form 1D chains like those in compounds **1**–**5**, their relative arrangement is modified. The angle between the benzene rings in TFBIB and the *ac* plane is about 60°, while the corresponding angle in **1**–**5** is almost 0°. Therefore, the inter-chain distance decreases to 3.80 Å. These modifications in the anion site make the donor arrangement different from those in crystals of **1**–**5**. There are several contacts between the anion moiety and donor molecules. The shortest distances between those atoms are 2.92, 3.17, and 2.62 Å for $Br^-\cdots H$, $I\cdots H$, and $F\cdots H$, respectively. The donor arrangement resembles the α-type.[10] The interplanar distance between the donor molecules is *ca.* 3.8 Å. There are several short $S\cdots S$ contacts (3.51–3.60 Å) between donor molecules (broken lines in Fig. 2).

$(ET)_2Cl_2$(BIDMB) 7. The crystal structure of **7** is quite different from the others as shown in Fig. 3. There is only one

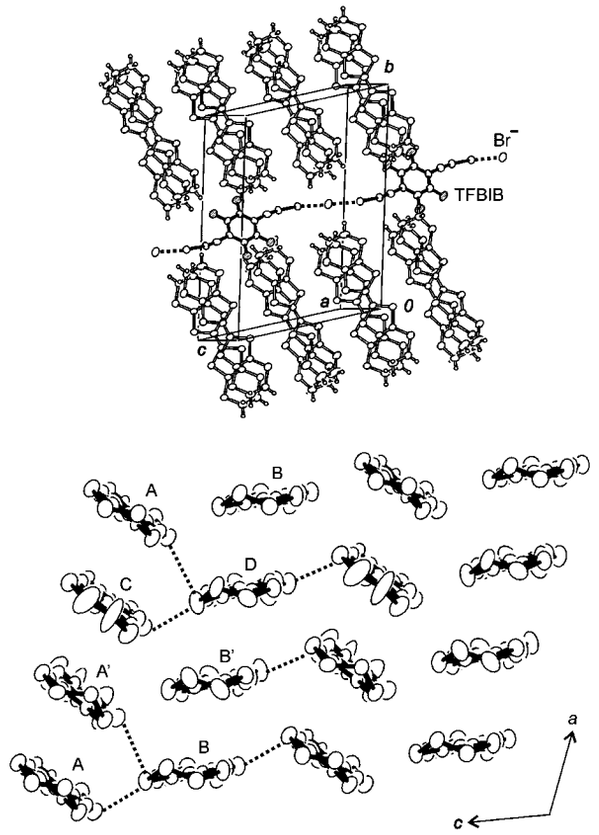

Fig. 2 Crystal packing (upper) and the α-type donor arrangement (lower) in **6**. Shaded atoms represent fluorine atoms. Hydrogen atoms in the lower figure are omitted for clarity. The benzene rings of TFBIB lean at an angle of 60° towards the *ac* plane.

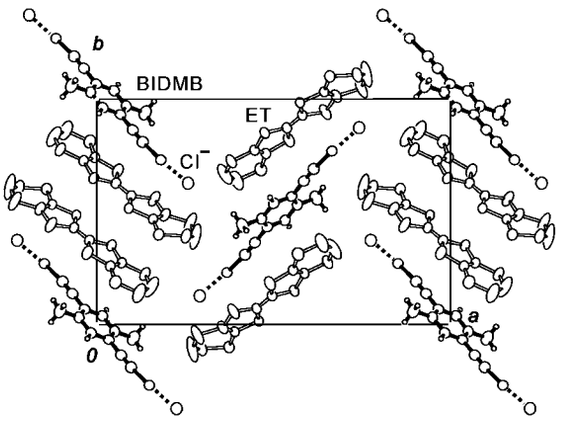

Fig. 3 Crystal structure of **7** viewed along the *c*-axis, where dashed lines represent $Cl^-\cdots I$. Hydrogen atoms on ET are omitted for clarity.

crystallographically independent donor molecule. There is no 1D chain based on the anions and the neutral molecules. Two ET molecules and one BIDMB molecule stack alternately to form 1D mixed columns. One BIDMB molecule is coordinated by two Cl anions. The $Cl^-\cdots I$ distance is 2.93 Å and the length of the $Cl^-\cdots$BIDMB$\cdots Cl^-$ unit is 17.9 Å. There are short interstack $Cl^-\cdots S$ contacts (3.43 and 3.52 Å) between the anion and ET molecule (the sum of the anion radius of Cl^- and the van der Waals radius of S is 3.55 Å).

Electrical resistivity

Fig. 4 and 5 show the temperature dependence of the resistivity parallel to the *ac* plane for $(ET)_3Cl$(*p*BIB) and the salts **1**–**5**. All these salts exhibit metallic behaviors down to 1.6 K. In both

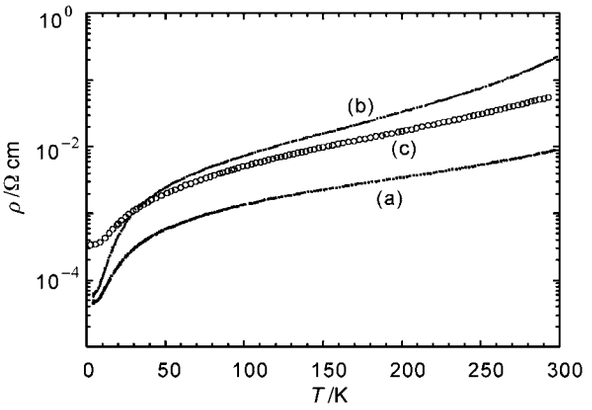

Fig. 4 Temperature dependence of the resistivity parallel to the *ac* plane of the Cl salts. (a) $(ET)_3Cl(pBIB)$; (b) $(ET)_3Cl(DFBIB)$; (c) $(ET)_3Cl(pBIB\text{-}d_4)$.

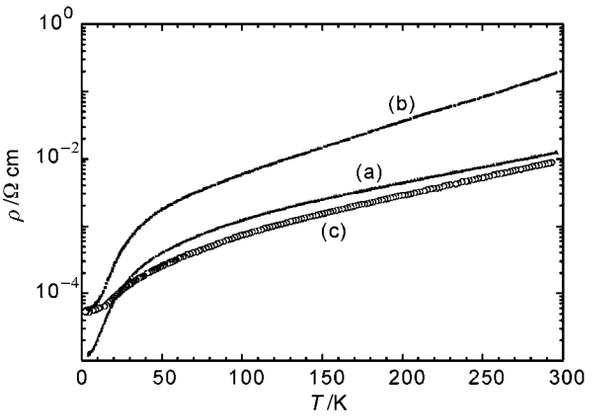

Fig. 5 Temperature dependence of the resistivity parallel to the *ac* plane of the Br salts. (a) $(ET)_3Br(pBIB)$; (b) $(ET)_3Br(DFBIB)$; (c) $(ET)_3Br(pBIB\text{-}d_4)$.

figures, it is notable that the room temperature resistivity of the salts with DFBIB is higher than other salts. The resistivity of **6** at 297 K is *ca.* 400 Ω cm and its temperature dependence exhibits activated behavior with an activation energy $E_a = 0.2$ eV The salt **7** is also semiconductive with room temperature resistivity of 10^4 Ω cm and $E_a = 0.3$ eV.

Discussion

The effects of the chemical modifications are observed in the structure of the anionic supramolecular assemblies, and the results are summarized in Table 2. The first effect is caused by introduction of substituents into the benzene ring of *p*BIB. Although there is no significant difference between *p*BIB-d_4 and *p*BIB salts, two fluorine atoms in the DFBIB molecule elongate the inter-chain distance (the definition is

Table 2 Important distances (Å) in the supramolecular assembly. Period denotes the distance between two halide ions that are connected by one *p*BIB derivative. For the definition of inter-chain distance, see Fig. 1

	$X^-\cdots I$ distance/Å	Inter-chain/Å	Period/Å
$(ET)_3Cl(pBIB)$	3.1285(6)	4.91	18.36
$(ET)_3Br(pBIB)$ **1**	3.2662(3)	4.92	18.63
$(ET)_3Cl(DFBIB)$ **2**	3.1343(2)	5.00	18.26
$(ET)_3Br(DFBIB)$ **3**	3.2722(4)	5.01	18.53
$(ET)_3Cl(pBIB\text{-}d_4)$ **4**	3.1512(6)	4.92	18.36
$(ET)_3Br(pBIB\text{-}d_4)$ **5**	3.2538(2)	4.93	18.62
$(ET)_3Br(TFBIB)$ **6**	3.1364(6)	4.10	18.21

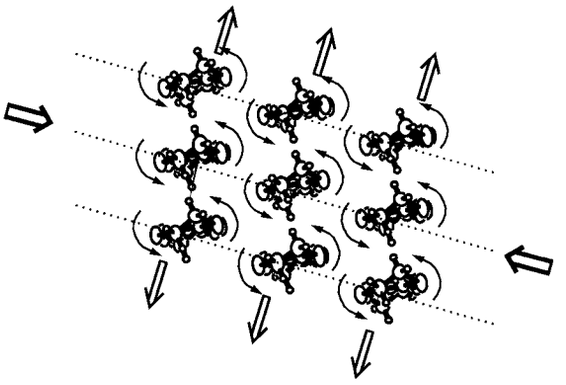

Fig. 6 Rotation of ET molecules (curved arrows) induced by the "anisotropic chemical pressure" (straight thick arrows). The dotted lines represent the direction of the 1D supramolecular assemblies.

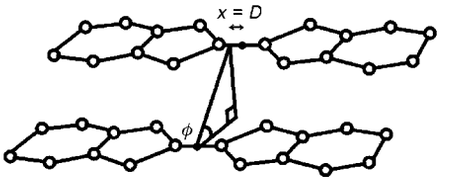

Fig. 7 Definition of ϕ and D. D represents the molecular slipping along the long axis. ϕ changes from 0° (side-by-side arrangement) to 90° (face-to-face stacking).

illustrated in Fig. 1) by steric repulsion. The inter-chain distance thus increases from 4.91 to 5.00 Å (Cl-*p*BIB *vs.* Cl-DFBIB (**2**)) or from 4.92 to 5.01 Å (Br-*p*BIB (**1**) *vs.* Br-DFBIB (**3**)). The bulkiness of the fluorine atoms also makes the DFBIB molecule distorted so that vacant space within the anion layer is reduced. The resulting S-shaped DFBIB molecule makes the $X^-\cdots DFBIB\cdots X^-$ periods shorter than those of $X^-\cdots pBIB\cdots X^-$.

In contrast to these reasonable changes, the $X^-\cdots I$ distances show a strange trend. The $X^-\cdots I$ distances are somewhat longer for these fluorine-substituted molecules (for example, the $X^-\cdots I$ distance is 3.128 Å for $Cl^-\cdots pBIB$ and 3.134 Å for $Cl^-\cdots DFBIB$). This fact seems to conflict with the electron-withdrawing nature of the fluorine atom because it is usually expected to draw the X^- ion closer to the iodine atom. Indeed, the $X^-\cdots I$ distance for $Br^-\cdots TFBIB$ is considerably shorter (3.14 Å) than that for $Br^-\cdots pBIB$ (3.27 Å). A simple comparison, however, is not possible because of the above-mentioned distortion of the supramolecular framework.

The second effect, caused by the replacement of the halide ions from Cl^- to Br^-, results in an increase of the $X^-\cdots pBIB\cdots X^-$ period. This increase in length ($= 18.63 - 18.36 = 0.27$ Å) is just twice as large as the increase of the $X^-\cdots I$ distance ($= 3.27 - 3.13 = 0.14$ Å). Therefore, it is natural to think that the increase of the period originates in the anion size difference. Compared to the apparent change of these intra-chain distances, the inter-chain distances are not sensitive to the $Cl^-\rightarrow Br^-$ substitution at all. For instance, the increase of the $X^-\cdots pBIB\cdots X^-$ period is about 1.5%, whereas the inter-chain distance remains almost constant (4.92→4.91 Å). This trend is also observed when DFBIB salts (**2** and **3**) or *p*BIB-d_4 salts (**4** and **5**) are examined.

In conclusion, it is clear that the chain period decreases in the order Br-*p*BIB > Cl-*p*BIB-d_4 (**4**) ≅ Cl-*p*BIB > Cl-DFBIB. The inter-chain distance, on the other hand, *increases* in a similar order (Br-*p*BIB ≅ Cl-*p*BIB-d_4 ≅ Cl-*p*BIB < Cl-DFBIB). These systematic deformations of the anion framework should distort the cell parameters and work on the donor moiety as "chemical pressure". It is probable that each donor molecule is rotated around its longitudinal molecular axis by the moment of force

Table 3 Intermolecular angle ϕ (degree) (see Fig. 7). The symbols **p**, **q**, **r1**, **r2**, **s1**, and **s2** denote the interrelation between donor molecules defined in Fig. 8. The ϕ values in **p**, **q**, **s1**, and **s2** directions decrease from Br-*p*BIB to Cl-DFBIB, whereas those in the **r1** and **r2** direction increase

	p	q	r1	r2	s1	s2
$(ET)_3Br(pBIB)$ **1**	80.64	82.18	23.49	22.57	14.68	16.31
$(ET)_3Cl(pBIB\text{-}d_4)$ **4**	78.94	80.05	24.49	23.84	13.90	15.45
$(ET)_3Cl(pBIB)$	78.63	79.69	24.69	24.04	13.82	15.39
$(ET)_3Br(DFBIB)$ **3**	79.57	78.98	23.80	22.00	14.38	14.86
$(ET)_3Cl(DFBIB)$ **2**	77.77	76.99	25.41	24.66	13.50	14.76

as shown in Fig. 6, because the chemical pressure is anisotropic and its direction is not parallel to any principal axes of the donor molecules. In order to clarify the influence of this anisotropic chemical pressure, we examined the relation between the intermolecular angles (ϕ) between donor molecules and the inter/intra-chain distances in the anion moiety. The definition of ϕ is illustrated in Fig. 7, along with the definition of the longitudinal displacement (D).

Table 3 lists the ϕ values in selected crystals. Due to the poor crystal quality, the data for **5** are omitted. For specification of the direction, we designate interrelations between two adjacent donor molecules as shown in Fig. 8. It should be noted that the 1D supramolecular assemblies (dotted lines) are parallel to the **r1** and **r2** interactions. From Table 3, it is clear that the anisotropic chemical pressure leads to systematic alteration of the ϕ values. For instance, the ϕ value in the **p** direction decreases from 80.64° (Br-*p*BIB) to 77.77° (Cl-DFBIB). The ϕ values in the **q**, **s1**, **s2** directions also decrease in the same order. On the contrary, those in the **r1** and **r2** directions (*i.e.* parallel to the 1D chain) *increase* in this order. These facts mean that the donor molecules are rotated as drawn in Fig. 6, and can be described as "anisotropic chemical pressure".

The rotation of the donor molecules should show effects on the intermolecular overlap integrals of the HOMO that forms the conduction band. The calculated overlap integrals are listed in Table 4. We confirmed that the D values do not show a large and systematic alteration compared to the ϕ values in the present system. In addition, the overlap integrals are not sensitive to the D values. Therefore, the influence from the D value is not considered in the following discussion.

According to the relation between the overlap integral and ϕ (Fig. 9), which was originally calculated by Mori *et al.*,[11] the overlap integral has a negative gradient against ϕ around

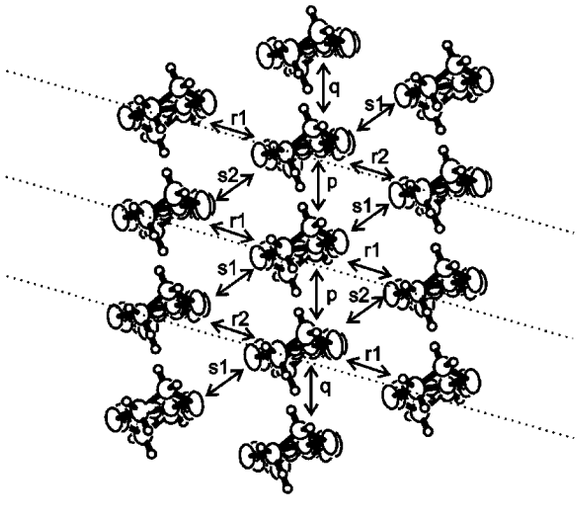

Fig. 8 Donor arrangement in **2** viewed along the longitudinal axes of the donor molecules. The dotted lines represent the 1D chains of Cl^- and DFBIB. Alphabetic letters indicate interrelations between donor molecules.

Table 4 Overlap integrals between HOMOs ($\times 10^3$). The magnitude of the overlaps systematically changes from Br-*p*BIB to Cl-DFBIB, which trend is consistent with the estimation from the ϕ value alteration

	p	q	r1	r2	s1	s2
$(ET)_3Br(pBIB)$ **1**	−5.70	−6.47	−4.41	−4.38	−1.30	−1.52
$(ET)_3Cl(pBIB\text{-}d_4)$ **4**	−5.38	−5.98	−4.85	−4.90	−1.09	−1.37
$(ET)_3Cl(pBIB)$	−5.15	−5.80	−5.03	−5.02	−1.07	−1.40
$(ET)_3Br(DFBIB)$ **3**	−5.60	−4.78	−4.97	−4.29	−1.03	−1.35
$(ET)_3Cl(DFBIB)$ **2**	−4.89	−5.65	−5.82	−5.33	−0.80	−1.10

$\phi = 80°$ (**p** and **q**), 25° (**r1** and **r2**), and 15° (**s1** and **s2**). This means that the increase of the ϕ values in the present system should always enhance the overlap (*i.e.* their absolute values), because all the overlap integrals are negative. When the direction of the donor rotation is considered, it is anticipated that the overlaps in the **p**, **q**, **s1**, and **s2** directions are attenuated in the order Br-*p*BIB > Cl-*p*BIB-d_4 ≅ Cl-*p*BIB > Cl-DFBIB, and the overlaps in **r1** and **r2** directions are enhanced in the same order (Br-*p*BIB < Cl-*p*BIB-d_4 ≅ Cl-*p*BIB < Cl-DFBIB). Indeed, Table 4 shows a clear trend in the overlap that can be explained by the molecular rotation. These changes are summarized in Fig. 10.

The changes of the overlap integrals affect the shape of the Fermi surface. Since the overlaps in $c-a$ (*i.e.* **p**, **q**) and $a+2c$ (*i.e.* **r1**, **r2**) directions are larger than those in the $2a+c$ (*i.e.* **s1** and **s2**) direction, the band dispersion is large along these directions. This 2D dispersion leads to a closed and elliptic cross section as shown in Fig. 11 (band filling is +5/6; in the calculation, the charges of the molecules are assumed to be equal to each other, which is supported by preliminary measurements of the Raman spectra[12]). Detailed calculations

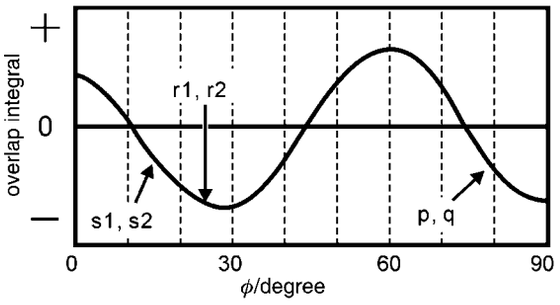

Fig. 9 ϕ-Dependence of the overlap integral between the HOMOs of two ET molecules. The D-dependence of this graph is very small.[11]

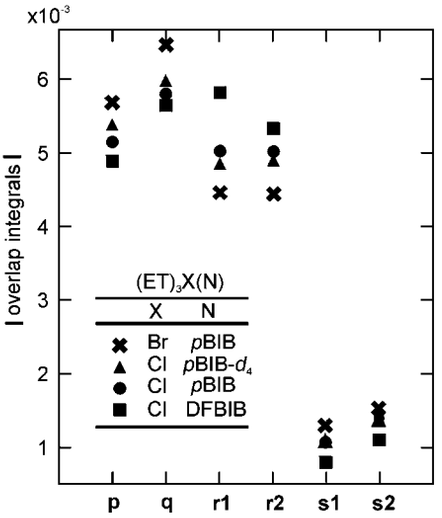

Fig. 10 Absolute values of the overlap integrals for $(ET)_3X(N)$ (X = anion, N = neutral molecule).

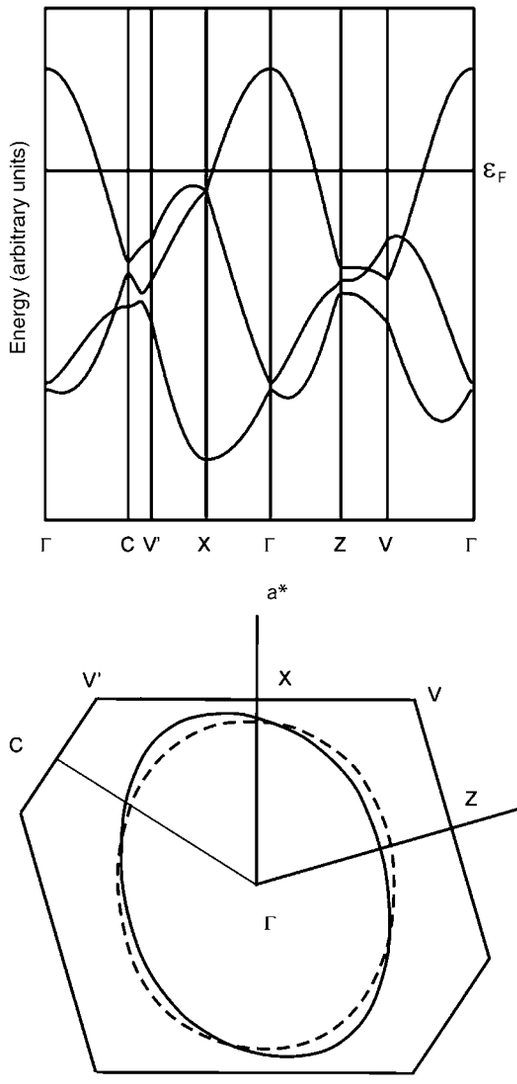

Fig. 11 Band structure (top) of **2** and the Fermi surfaces (bottom) of **2** (solid line) and **1** (broken line).

have indicated that the ellipse would become slender when the overlaps in $c-a$ or $2a+c$ directions are attenuated or those in the $a+2c$ direction are enhanced. Therefore, the anisotropy of the Fermi surface increases from Br-*p*BIB to Cl-DFBIB through the attenuation of the overlaps in the **p**, **q**, **s1**, and **s2** directions as well as the enhancement of those in the **r1** and **r2** directions. The ratio of the long axis to the short axis of the ellipse then ranges from 1.22 for **1** to 1.39 for **2** (Fig. 11, Table 5). This is the result of the "anisotropic chemical pressure".

In contrast to the systematic changes in the crystals **1**–**5**, the structure of the salt **6** is significantly different. The 1D supramolecule is basically sustained, but the benzene rings are no longer parallel to the *ac* plane and lean by 60° (Fig. 2). The donor arrangement is also changed from the β-type to the α-type. The reason for this discontinuous structural change is not very clear, but one of the plausible answers can be found in

Table 5 Ratio of the long axis to the short one for the elliptic cross section of the Fermi surface

	Long axis/short axis
$(ET)_3Br(pBIB)$ **1**	1.22
$(ET)_3Cl(pBIB\text{-}d_4)$ **4**	1.26
$(ET)_3Cl(pBIB)$	1.29
$(ET)_3Br(DFBIB)$ **3**	1.29
$(ET)_3Cl(DFBIB)$ **2**	1.39

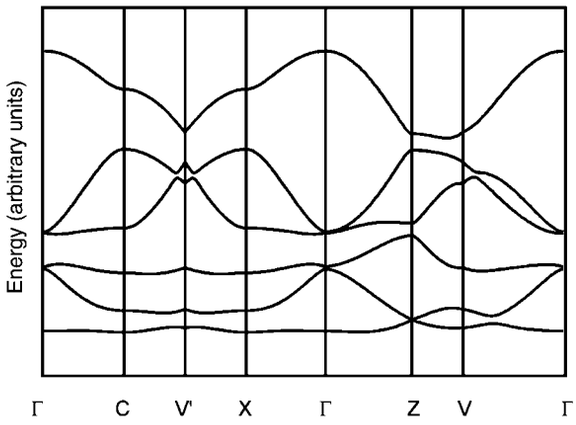

Fig. 12 Calculated band structure of the salt **6**. The chemical potential of this salt is located in the middle of the gap between the top sub-band and the second one. The names of the points in the reciprocal space are the same as drawn in Fig. 11.

the lack of the hydrogen bond between the benzene ring and halide ions observed in the *p*BIB or DFBIB systems. Since the TFBIB molecule does not possess any hydrogen atoms on its benzene ring, the inter-chain interaction is no longer attractive but is repulsive due to the electrostatic repulsion between fluorine atoms and halide ions.

Another possibility can also be found in the excess unit area of the anion layer: the unit cell of the anion layer (*i.e. ac* plane) in the crystals **1**–**5** occupies 90 Å^2 which means 30 Å^2 for one ET molecule. Compared to the normal value (*ca.* 25 Å^2 for one ET molecule) which is estimated from the previously reported data of other ET salts, this anion area is extremely large. The donor molecules are thus inclined about 40° in the crystals **1**–**5**, in order to compensate for this too large anion area. If the anionic supramolecule based on TFBIB takes the same flat structure as in **1**–**5**, the anion area increases further and the ET molecules have to be inclined more. Therefore, it is reasonable to think that the benzene rings are rotated to reduce anion area, so that the ET molecules need not take an unstably inclined position. Indeed, the unit area of the *ac* plane in the crystal **6** is 75 Å^2 (25 Å^2 for one ET molecule) and the donor molecules are not inclined against the anion layer any longer (the angles between the longitudinal axes of the donor molecules and the normal of the anion layer are less than 15°). In this system, therefore, the structural alteration of the anion layer seems to induce the change of the donor arrangement.

A bond length examination[13] suggests that there occurs a charge separation among the donor molecules in the crystal **6** [four donor molecules (A, A′, B, and B′) possesses *ca.* +0.3 positive charge and other two (C and D) possesses *ca.* +0.5]. Because the charge separation is small, however, the tight-binding band calculation for **6** is performed with an assumption that the formal charges are equal to each other (+1/3). The calculation reveals that crystal **6** is a band insulator with a 5/6-filled HOMO band (Fig. 12). This result is consistent with the semiconductive temperature dependence of the resistivity.

As for the structure of crystal **7**, two methyl groups in the BIDMB molecule are too sterically bulky to form a flat anion layer as in **1**–**5** or **6**, and thus the BIDMB molecule only forms a discrete anion complex.

Summary

We have described structural and physical properties of new ET-based cation radical salts containing di- or tetra-substituted *p*BIB derivatives. Five new salts **1**–**5** are metallic down to the lowest temperature, while others are semiconductive. These electrical behaviors can be explained by the tight-binding band calculations based on the crystal structure data. In the difluoro-

Table 6 Conditions for crystal growth

	1	2	3	4	5	6	7
Solvent	CB[a] : MeOH 4 : 1	CB : MeOH 9 : 1	CB : MeOH 19 : 1	CB : MeOH 9 : 1	CB : MeOH 19 : 1	CB : MeOH 9 : 1	BN[c] : MeOH 9 : 1
Donor	ET	ET	ET	ET	ET	ET	ET
Neutral molecules	*p*BIB	DFBIB	DFBIB	*p*BIB-d_4	*p*BIB-d_4	TFBIB	BIDMB
Supporting electrolyte	TPPBr[b]	TPPCl	TPPBr	TPPCl	TPPBr	TPPCl	TPPCl
Current/μA	0.6	2.0	0.5	0.3	0.5	1.0	2.0
Time/days	8	6	8	13	13	8	8
Crystal shape	Plate	Block	Block	Block	Plate	Block	Block

[a]CB = chlorobenzene. [b]TPP = tetraphenylphosphonium. [c]BN = benzonitrile.

substitutions and halide ion replacement, we could reveal the systematic substitution effect on the crystal structure, which works as an "anisotropic chemical pressure". Their 2D Fermi surfaces are anisotropically affected by this chemical pressure. In this series of materials, unfortunately, the change of the electronic structure is not enough to induce drastic (electric) transitions. This is in contrast to the cases of the deuteration for $(DMe\text{-}DCNQI)_2Cu$[7] and $(ET)_2CuBr[N(CN)_2]$[8] where the structural changes are much smaller than those in the present system. The strategy here we have demonstrated, however, would provide an effectual means to tune the electronic structure and be made the most of in other sensitive systems. On the other hand, the tetrafluoro-substitution has induced a completely different type of donor arrangement. This discontinuous change implies the importance of the hydrogen bonds and the balance between the area of the anion layer and that of the donor layer for the crystal formation. All these results pave the way for a conceptual advance of crystal engineering in the field of molecular conductors.

Experimental

Synthesis

ET[14] and *p*BIB[3] were synthesized according to the literature procedures. The iodine-containing neutral molecules were synthesized in the same manner as in the literature[3,15] from 1,4-dibromo-2,5-difluorobenzene, 1,4-dibromotetrafluorobenzene, 1,4-dibromo-2,5-dimethylbenzene and 1,4-dibromobenzene-d_4. Single crystals were grown electrochemically in an H-shaped 20 ml cell under an argon atmosphere at constant current at 20 or 45 °C. The donor molecule, the neutral molecule and a supporting electrolyte were dissolved in chlorobenzene, 1,1,2-trichloroethane or benzonitrile. (TPP)X (TPP = tetraphenylphosphonium, X = Cl, Br) was used for the supporting electrolyte and anion source. Detailed conditions are given in Table 6.

Crystal structure

Crystal data were collected using a Weissenberg-type imaging plate (DIP320, MAC Science) or an automatic four-circle diffractometer (MXC18, MAC Science) with graphite-monochromated Mo-Kα ($\lambda = 0.71070$ Å) radiation at room temperature. ω–2θ scans were employed for data collection and Lorentz and polarization corrections were applied in the four-circle diffractometer measurements. The crystal structures were solved by the direct method and refined by the full-matrix least-squares procedure. For **1**, **3**, and **5** the refinement was performed using SHELXL-93.[16] For other salts, calculations were performed with the use of the teXsan crystallographic software package from Molecular Structure Co.[17] When the four-circle diffractometer was used, analytical absorption correction was also carried out. In the case of the imaging plate, the absorption correction was included in the scaling process of the image data. The temperature factors were refined anisotropically for the non-hydrogen atoms. All hydrogen atoms were located at calculated positions with fixed isotropic contributions.

Table 7 The exponents ζ and the ionization energies ε/eV for atomic orbitals

Atom	Orbital	ζ	ε/eV
S	3s	1.817	−19.6
	3p	1.817	−13.3
C	2s	1.625	−21.4
	2p	1.625	−11.4
H	1s	1.30	−13.6

Band calculation

The overlap integrals (S) between HOMOs of adjacent donor molecules were calculated on the basis of the extended Hückel MO method. The semiempirical parameters for Slater-type atomic orbitals are given in Table 7.[18] The band structures and the shapes of the Fermi surfaces were obtained by the tight-binding method, using the transfer integral (t) from the approximation $t = ES$, where E is a constant whose order is that of the energy level of the HOMO (~10 eV).

Electrical resistivity

The measurements of the temperature dependence of resistivity were carried out by the standard four-probe dc method. Gold leads (10 μm diameter) were attached to the sample with carbon paste.

Acknowledgements

The authors are grateful to Dr Makoto Inokuchi of the Science University of Tokyo in Yamaguchi and Professor Kyuya Yakushi of the Institute for Molecular Science for the measurement of the Raman spectra.

References

1 S. Kagoshima, R. Kato, H. Fukuyama, H. Seo and H. Kino, in *Advances in Synthetic Metals – Twenty Years of Progress in Science and Technology*, eds. P. Bernier, S. Lefrant and G. Bidan, Elsevier, Amsterdam, 1999, p. 262.

2 (*a*) T. Imakubo, H. Sawa and R. Kato, *J. Chem. Soc., Chem. Commun.*, 1995, 1667; (*b*) T. Imakubo, H. Sawa and R. Kato, *Synth. Met.*, 1995, **73**, 117.

3 H. M. Yamamoto, J. Yamaura and R. Kato, *J. Am. Chem. Soc.*, 1998, **120**, 5905.

4 D. Jérome, A. Mazaud, M. Ribault and K. Bechgaad, *J. Phys.*, 1980, **41**, L95.

5 J. M. Williams, A. M. Kini, H. H. Wang, K. D. Carlson, U. Geiser, L. K. Montgomery, G. J. Pyrka, D. M. Watkins, J. M. Kommers, S. J. Boryschuk, A. V. S. Crouch, W. K. Kwok, J. E. Schirber, D. L. Overmyer, D. Jung and M.-H. Whangbo, *Inorg. Chem.*, 1990, **29**, 3272.

6 (*a*) R. Kato, H. Kobayashi and A. Kobayashi, *J. Am. Chem. Soc.*, 1989, **111**, 5224; (*b*) R. Kato, S. Aonuma and H. Sawa, *Mol. Cryst. Liq. Cryst.*, 1996, **284**, 183.

7 (*a*) S. Hünig, K. Sinzger, M. Jopp, D. Bauer, W. Bietsch, J. U. von Schütz and H. C. Wolf, *Angew. Chem., Int. Ed. Engl.*, 1992, **31**, 859; (*b*) K. Sinzger, S. Hünig, M. Jopp, D. Bauer, W. Bietsch,

J. U. von Schütz, H. C. Wolf, R. K. Kremer, T. Metzenthin, R. Bau, S. I. Khan, A. Lindbaum, C. L. Lengauer and E. Tillmanns, *J. Am. Chem. Soc.*, 1993, **115**, 7696; (*c*) R. Kato, H. Sawa, S. Aonuma, M. Tamura, M. Kinoshita and H. Kobayashi, *Solid State Commun.*, 1993, **85**, 831; (*d*) S. Aonuma, H. Sawa and R. Kato, *J. Chem. Soc., Perkin Trans. 2*, 1995, 1541; (*e*) R. Kato, *Bull. Chem. Soc. Jpn.*, 2000, **73**, 515.

8 A. Kawamoto, H. Taniguchi and K. Kanoda, *J. Am. Chem. Soc.*, 1998, **120**, 10984.

9 T. Mori, *Bull. Chem. Soc. Jpn.*, 1998, **71**, 2509.

10 T. Mori, H. Mori and S. Tanaka, *Bull. Chem. Soc. Jpn.*, 1999, **72**, 179.

11 T. Mori, A. Kobayashi, Y. Sasaki, H. Kobayashi, G. Saito and H. Inokuchi, *Bull. Chem. Soc. Jpn.*, 1984, **57**, 627.

12 The Raman spectra for **1** and **2** were measured at room temperature and 4.2 K. For both salts, only one vibrational mode was observed in the region of ν_3 that is sensitive to the oxidation state of ET (see: J. Moldenhauer, Ch. Horn, K. I. Pokhodnia, D. Schweitzer, I. Heinen and H. J. Keller, *Synth. Met.*, 1993, **60**, 31). This is why we are convinced of the equal potential of ET molecules.

13 P. Guionneau, C. J. Kepart, G. Bravic, D. Chasseau, M. R. Truter, M. Kurmoo and P. Day, *Synth. Met.*, 1997, **86**, 1973.

14 (*a*) M. Mizuno, A. F. Garito and M. Cava, *J. Chem. Soc., Chem. Commun.*, 1978, 18; (*b*) N. Svenstrup and J. Becher, *Synthesis*, 1995, 215.

15 S. Takahashi, Y. Kuroyama, K. Sonogashira and N. Hagihara, *Synthesis*, 1980, 627.

16 G. M. Sheldrick, *Program for the Refinement of Crystal Structures*, University of Göttingen, Germany, 1993.

17 Y. Kai, *Nippon Kessho Gakkaishi.*, 1991, **33**, 295.

18 E. Canadell, I. E.-I. Rachidi, S. Ravy, J. P. Pouget, L. Brossard and J. P. Legros, *J. Phys. Fr.*, 1989, **50**, 2967.